Since January 2020 Elsevier has created a COVID-19 resource centre with free information in English and Mandarin on the novel coronavirus COVID-19. The COVID-19 resource centre is hosted on Elsevier Connect, the company's public news and information website.

Computers in Biology and Medicine 133 (2021) 104383

Contents lists available at ScienceDirect

Computers in Biology and Medicine

journal homepage: http://www.elsevier.com/locate/compbiomed

Promising phytochemicals of traditional Himalayan medicinal plants against putative replication and transmission targets of SARS-CoV-2 by computational investigation

Jagadish Natesh [a,b], Priya Mondal [a,b], Bhavjot Kaur [a], Abdul Ajees Abdul Salam [c], Srikaa Kasilingam [a], Syed Musthapa Meeran [a,b,*]

[a] Department of Biochemistry, CSIR-Central Food Technological Research Institute, Mysore, 570 020, India
[b] Academy of Scientific and Innovative Research (AcSIR), Ghaziabad, 201 002, India
[c] Department of Atomic and Molecular Physics, Centre for Applied Nanosciences, Manipal Academy of Higher Education, Manipal, 576 104, India

ARTICLE INFO

Keywords:
COVID-19
SARS-CoV-2
Molecular docking
Himalayan medicinal plants

ABSTRACT

Background: Identification and repurposing of therapeutic and preventive strategies against COVID-19 are rapidly undergoing. Several medicinal plants from the Himalayan region have been traditionally used to treat various human disorders. Thus, in our current study, we intended to explore the potential ability of Himalayan medicinal plant (HMP) bioactives against COVID-19 using computational investigations.

Methods: Molecular docking was performed against six crucial targets involved in the replication and transmission of SARS-CoV-2. About forty-two HMP bioactives were analyzed against these targets for their binding energy, molecular interactions, inhibition constant, and biological pathway enrichment analysis. Pharmacological properties and potential biological functions of HMP bioactives were predicted using the ADMETlab and PASS webserver respectively.

Results: Our current investigation has demonstrated that the bioactives of HMPs potentially act against COVID-19. Docking results showed that several HMP bioactives had a superior binding affinity with SARS-CoV-2 essential targets like $3CL^{pro}$, PLpro, RdRp, helicase, spike protein, and human ACE2. Based on the binding energies, several bioactives were selected and analyzed for pathway enrichment studies. We have found that selected HMP bioactives may have a role in regulating immune and apoptotic pathways. Furthermore, these selected HMP bioactives have shown lower toxicity with pleiotropic biological activities, including anti-viral activities in predicting activity spectra for substances.

Conclusions: Current study results can explore the possibility of HMPs as therapeutic agents against COVID-19.

1. Introduction

Coronavirus disease (COVID-19) pandemic has paralyzed societal and economic conditions across the world. It is one of the life-threatening disease for which no specific preventive or curative treatment has been foolproof so far. According to WHO statistics, by the end of March 2021, COVID-19 has infected more than 123 million people worldwide and caused more than 2.71 million mortality. COVID-19 is caused by severe acute respiratory syndrome coronavirus 2 (SARS-CoV-2), which belongs to the β coronavirus family of enveloped positive-sense RNA viruses [1]. The SARS-CoV-2 viral life cycle involves infection of host cells, viral gene translation (non-structural proteins), and viral genome replication [2]. A comprehensive understanding of the viral life cycle provides critical viral and host factors that offer valuable targets for developing a therapeutic strategy against COVID-19.

The viral life cycle initiates with the entry of SARS-CoV-2 into the host cell. The entry of the virus takes place through the host cell receptor interaction by the SARS-CoV-2 spike protein. Spike protein is a vital structural protein that recognizes the human angiotensin-converting enzyme 2 (ACE2) receptor and facilitates viruses' binding to the host cells [3]. Spike protein is composed of S1 and S2 subunits, wherein the S1 subunit recognizes the ACE2 receptor and binds it, following which

* Corresponding author.Laboratory of Cancer Epigenetics, Department of Biochemistry, CSIR-Central Food Technological Research Institute (CSIR-CFTRI), Mysore, 570 020, India.
E-mail addresses: s.musthapa@cftri.res.in, syedmusthapa@gmail.com (S.M. Meeran).

https://doi.org/10.1016/j.compbiomed.2021.104383
Received 2 February 2021; Received in revised form 25 March 2021; Accepted 2 April 2021
Available online 20 April 2021

S2 subunit helps the viral membrane fusion with the host membrane resulting in the release of the viral genome into the host cell [4,5]. Intriguingly, the spike protein binding affinity of SARS-CoV-2 with ACE2 receptor is ten to twenty-fold higher than SARS-CoV, which might have contributed to the higher infection and transmission of SARS-CoV-2 in comparison with previous coronavirus infections [6,7].

After the viral genome's release into the host cell, it leads to complex viral gene expressions. Initially, ORF1a and ORF1b from the viral genome is translated into pp1a and pp1ab polyproteins. Two vital proteins process these polyproteins, i.e., 3-chymotrypsin-like proteinase ($3CL^{pro}$)/main proteases (M^{pro}) and papain-like protease (PLpro), into several non-structural proteins (nsps), which are involved in SARS-CoV-2 genome replication. Several nsps, including nsp12, i.e., RNA-dependent RNA polymerase (RdRp), and nsp13, i.e., helicase, are engaged in the SARS-CoV-2 viral replication machinery [2]. Thus, $3CL^{pro}$, PLpro, RdRp, helicase, spike protein, and human ACE2 are the crucial proteins involved in the SARS-CoV-2 lifecycle and might be valuable targets for intervention of COVID-19.

Host response against SARS-CoV-2 has a significant influence on the severity of COVID-19. Cytokine production, the hyperinflammatory response against the virus, and comorbidities will significantly impact COVID-19 disease progression [8]. Fever, cough, sore throat, headache, fatigue, breathlessness, diarrhea, muscle pain, and sputum production are commonly observed symptoms in COVID-19 patients [9]. On the other hand, in the advanced stages of COVID-19, patients suffer from acute respiratory distress syndrome, loss of speech or movement, chest pain or pressure, and severe cardiac injury, leading to death. Extensive research is going on different anti-viral drugs, vaccines, and therapeutic formulations to treat the SARS-CoV-2. Currently, a sequential clinical trial of anti-viral drugs in combination has been investigated against COVID-19. The combination of nitazoxanide, ribavirin, and ivermectin is under phase III clinical trials against COVID-19 (Clinical trial# NCT04392427). Furthermore, the FDA-approved remdesivir is the first emergency drug for treating hospitalized COVID-19 patients over the age of 12. However, there is a lack of confidence in the effectiveness of drugs or vaccines against COVID-19, even when the number of new cases, new viral strains, and mortality rates are still increasing globally.

Several countries, including India, have focused on their ancient practices to overcome this problem. '*Ayurveda*' is one of the traditional medicines that have been the source of remedies for numerous diseases, including viral infection, flu, cold, etc. Also, the Indian Materia Medica comprises around two thousand natural origin drugs, nearly most of them can be obtained from diverse traditional systems and folklore practices [10]. The Himalayan region is one of the oldest and wealthiest medicinal plant biodiversity repositories among different world regions. The geographical features, including altitude, ecology, topography, and climatic conditions, are making this region home to more than 8,000 species of vascular plants, of which 1,748 are known for their medicinal properties. These higher altitude plants have played essential roles in the lives of tribal peoples by acting as herbal medicines. From ancient times, different parts of these altitude medicinal plants have been used as curative agents, especially for cold, cough, fever, bronchitis, and asthma, either alone or in combination with common medicinal plants [11].

Therefore, the Himalayan ayurvedic plant's formulation can be used alone or tested with an approved drug to treat COVID-19. The computational biology approach is required to predict the effective drugs or formulation from Himalayan medicinal plants (HMPs) against COVID-19. In the current study, we have selected HMP bioactives, which are traditionally used for cold, cough, fever, bronchitis, and asthma, and investigated their potentialities against COVID-19 by targeting the viral proteins involved in replication, maturation, and transmission to the host using computational approaches. Further, the therapeutic roles of the selected HMP bioactives were also analyzed using biological pathway enrichment analysis.

2. Materials and methods

2.1. Selection of bioactives from Himalayan medicinal plants

The selection of HMPs was based on a thorough search of the existing traditional use of the different parts of the plants against respiratory-related viral diseases, as summarized in Supplementary Table S1. The ethnopharmacological use of selected HMPs was well documented and found a lack of scientific validation. Therefore, in the current study, we identified forty-two bioactives from seventeen HMPs for the computational investigation against the potential targets of SARS-CoV-2 as summarized in Supplementary Table S2. Further, the potential bioactives were selected based on the highest binding affinity towards target proteins of SARS-CoV-2. The three-dimensional structures of standard drugs and HMP bioactives were retrieved from the PubChem database (https://pubchem.ncbi.nlm.nih.gov/). Several anti-retroviral proteases, RdRp, and human ACE2 inhibitors (Darunavir, remdesivir, ritonavir, losartan, and enalapril) were selected as the standard drugs for docking analysis against SARS-CoV-2 target proteins (Supplementary Table S3). Ligand molecules were converted into Protein Data Bank (PDB) format using Open Babel software (The Open Babel Package, version 2.3.1; http://openbabel.org) and were prepared for docking by converting them into PDBQT format using AutoDock Tools [12].

2.2. Protein preparation

The three-dimensional coordinates of the targets of SARS-CoV-2 molecules 6LU7 ($3CL^{pro}$), 7JRN (PLpro), 6M71 (RdRp), 6ZSL (helicase), 6W41 (spike protein), and 1R42 (ACE2) were retrieved from PDB [13–17]. These SARS-CoV-2 target proteins have been used in several investigations to identify therapeutics against COVID-19 [13,18–21]. The protein molecules were processed by removing crystallographic water molecules, adding polar hydrogens, followed by stabilizing the charges as demonstrated earlier [22,23]. Finally, the three-dimensional coordinates were converted into PDBQT format using ADT [12].

2.3. Molecular docking

SARS-CoV-2 $3CL^{pro}$, PLpro, RdRp, helicase, spike protein, and human ACE2 receptor were used as the target molecules for docking with the bioactives from HMPs. Molecular docking was carried out using AutoDock Vina [24]. Grid boxes were created around the active sites of SARS-CoV-2 $3CL^{pro}$, PLpro, RdRp, helicase, and the interacting crucial residues of the SARS-CoV-2 spike protein-human ACE2 receptor complex using Autodock tools with dimensions relative to the ligands (XYZ) with a resolution of 1 Å [22,23,25]. Each docking calculation was performed three-times using different seeds and retaining the remaining values as default. Protein-ligand interactive models were selected based on the binding energies (BEs), the potential hydrogen bonds (H-bonds), and hydrophobic interactions. Protein-ligand interaction profiler (PLIP) (https://projects.biotec.tu-dresden.de/plip-web/plip/) was used to determine H-bonds and non-bonded interactions. 3D stereo figures of protein-ligand interactions were computed using PyMOL (https://pymol.org/2). Further, the inhibition constant (Ki) for HMP bioactives with SARS-CoV-2 protein targets was calculated using the following equation [23,26].

$$Ki = 10^{(\text{Binding energy}/1.366)}$$

2.4. Biological pathway enrichment analysis

SwissTargetPrediction web server (http://www.swisstargetprediction.ch) was used to predict the top fifteen human protein targets for each of the selected bioactives of HMPs [27]. Ninety-three human

Table 1
Binding energies (BEs) (kcal/mol) of selected bioactives from the Himalayan medicinal plants against SARS-CoV-2 3CL^{pro} and PLpro, along with their hydrogen bonding (H-bond), hydrophobic interactions (HP), and inhibition constant (Ki), are shown. The bioactive compounds' names are displayed in **boldface**, and the botanical plant names are given in *italics*.

Himalayan medicinal plants and their bioactives	SARS-CoV-2 3CL^{pro}				SARS-CoV-2 PLpro			
	BE	H-Bond	HP	Ki (μM)	BE	H-Bond	HP	Ki (μM)
Remdesivir*	−8.3	Leu141, Gly143, His163, Glu166	Thr25, Thr26, Leu27, His41, Met49, Met165, Glu166, Gln189	0.84	−6.2	Lys105, His272, Lys274	Trp106, Asp286, Ala288, Leu289	28.92
Candibirin H *Heracleum candicans* Wall.	−9.2	Asn142, Gly143, Cys145, His163	His41, Met165, Glu166, Gln189	0.18	−7.0	His272, Ala288, Leu289	Lys274, Asp286	7.51
Candibirin G *Heracleum candicans* Wall.	−9.1	Gly143, Cys145, Glu166	Leu27, His41, Met165, Gln189	0.22	−6.6	Lys274	Trp106, Thr265, His272, Asp286	14.74
Catechin 5-O-gallate *Acacia nilotica*	−8.2	Thr26, Leu141, Gly143, Glu166	Thr25, Leu27, His41, Cys145, Met165, Arg188	0.99	−7.1	Trp106, Asn109, Cys270, His272, Asp286, Ala288	Trp106, Leu289	6.34
Hypericin *Hypericum perforatum* L.	−8.8	Gly143, Cys145, His163, Gln189	Met49, Phe140, Ser144, Glu166	0.36	−7.6	Cys270, Lys274	Trp106, Gly271, His272, Asp286	2.73
Pseudohypericin *Hypericum perforatum* L.	−8.5	Gly143, Cys145, His163, Glu166, Gln189	Ser144, Glu166	0.60	−7.4	Trp106, Thr265, His272, Lys274	Gly266, His272, Asp286	3.83

protein targets were set after redundancy removal (Supplementary Table S4). Besides, one hundred seventy-two human protein targets of the SARS-CoV-2 were chosen from the literature [28,29]. Pathway enrichment analysis was performed by the Enrichr database [30,31]. Enrichr displayed results according to *p*-values computed using the Fisher exact test for pathway and database enrichment for Kyoto Encyclopedia of Genes and Genomes (KEGG) pathways and VirusMint database. VirusMint (https://maayanlab.cloud/Harmonizome/resource/Virus+MINT) is a database that contains all the protein interactions between the virus and human proteins [32]. Further, the Revigo web server (http://revigo.irb.hr/) was used to remove redundancy from the list of Gene Ontology (GO) biological processes ($p < 0.001$) obtained from Enrichr. Results were plotted using a scatterplot on the Revigo database.

2.5. Evaluation of ADME/Toxicity prediction

ADMETlab web server (http://admet.scbdd.com) was used to predict

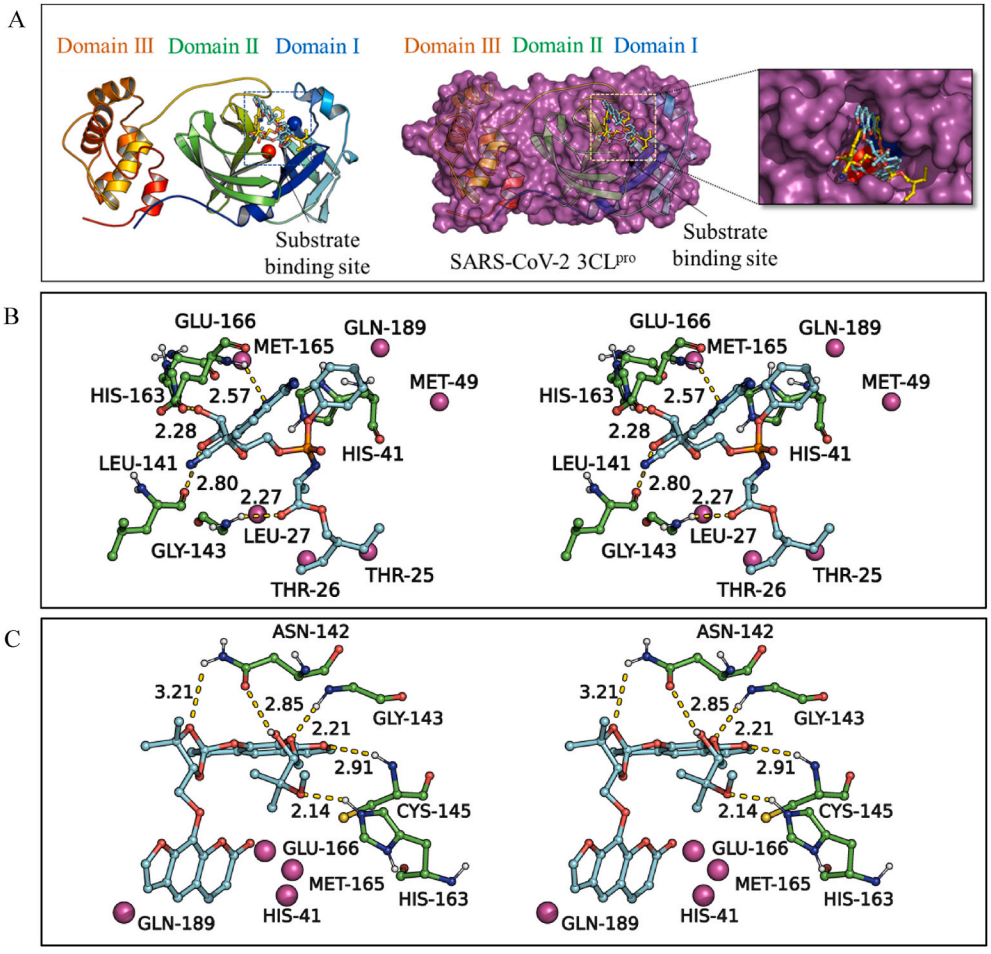

Fig. 1. (A) Secondary structural representation of SARS-CoV-2 3CL^{pro} (cartoon and surface representation) consists of domain I (blue), domain II (green), and domain III (orange). The His41-Cys145 catalytic dyad is shown in the sphere and colored red and blue, respectively. The substrate-binding site is highlighted in a square box, docked molecules remdesivir (yellow) and candibirin H (sky blue) are shown in the ball-and-stick model, and its close-up view is shown in the rightmost panel. (B–C) 3D stereo figures demonstrating molecular interactions of SASR-CoV-2 3CL^{pro} (PDB ID: 6LU7) with remdesivir (B) and bioactive from HMP candibirin H (C) are shown. The 3CL^{pro} residues making H-bond are shown in the ball-and-stick model, and carbon atoms are colored green. The 3CL^{pro} residues, which make hydrophobic interactions, are shown in the sphere (purple). H-bond interactions are shown in dotted lines, and the corresponding distances (Å) are marked. The remdesivir and candibirin H are also shown in the ball-and-stick model, and the carbon atoms are colored green and cyan, respectively. The oxygen and nitrogen are colored red and blue for both bioactives.

the absorption, distribution, metabolism, excretion, and toxicity of selected bioactives from HMP. The numerological values was interpreted by the qualitative units based on the ADMETlab server explanation.

2.6. Estimation of biological activity

PASS (Prediction of Activity Spectra for Substances)-Way2Drug server (http://www.pharmaexpert.ru/passonline/) was used to predict the biological activity of the selected HMP bioactives. PASS helps to predict the potentially active or inactive ligands based on their Pa (close to one for active compound) and Pi (should be close to zero for inactive compounds) values.

3. Results and discussion

3.1. Molecular docking

Our current study intended to identify potential HMP bioactives against the replication, maturation, and transmission targets of SARS-CoV-2. In this study, we have utilized molecular docking analysis to identify therapeutic agents from HMPs against COVID-19. Molecular docking is a versatile tool that predicts the binding efficiency and interactions between the therapeutic compounds and protein targets. SARS-CoV-2 viral life cycle provides several therapeutic targets to develop treatment options against the virus. Among these, targeting replication, maturation, and transmission of the virus hold great potential. Thus, we have chosen SARS-CoV-2 $3CL^{pro}$, PLpro, RdRp, and helicase as replication and maturation targets. SARS-CoV-2 spike protein and human ACE2 receptor were chosen as transmission targets to identify potential bioactives from HMPs that can probably inhibit SARS-CoV-2 using molecular docking analysis.

3.1.1. HMP bioactives with SARS-CoV-2 replication and maturation targets

Initially, we performed molecular docking analysis with standard anti-retroviral drugs with replication and maturation targets. Among the standard drugs, remdesivir is the FDA recommended emergency use authorization (EUA) drug for SARS-CoV-2 treatment, which had superior binding affinities towards $3CL^{pro}$ (BE: -8.3 kcal/mol), PLpro (BE: -6.2 kcal/mol), RdRp (BE: -7.1 kcal/mol), and helicase (BE: -8.0 kcal/mol). The results are summarized in Supplementary Table S3. After that, we obtained BEs of HMP bioactives against these targets. Among HMP bioactives, candibirin H had the highest binding affinity with $3CL^{pro}$ (−9.2 kcal/mol) and helicase (−9.1 kcal/mol), whereas hypericin had a higher binding affinity with PLpro (−7.6 kcal/mol) and RdRp (−8.9 kcal/mol). Based on the BEs of standard drug and HMP bioactives, we set the cut-off BE of −8.0 kcal/mol for $3CL^{pro}$, −6.5 kcal/mol for PLpro, −8.0 kcal/mol for RdRp, and −7.5 kcal/mol for helicase. Based on the cut-off BEs, potential HMP bioactives were further narrowed for protein-ligand interaction studies and biological pathway enrichment analysis. The criteria selected were based on (i) the cut-off BEs, and (ii) having a higher binding affinity towards all the targets of SARS-CoV-2. Five HMP bioactives such as candibirin H, candibirin G, catechin 5-*O*-gallate, hypericin, and pseudohypericin yielded superior BE values against SARS-CoV-2 replication and maturation targets, and their interactions with protein targets were analyzed.

SARS-CoV-2 $3CL^{pro}$ is an attractive drug target as it plays an essential role in the proteolytic maturation of pp1a and pp1ab polyproteins involved in the replication and transcription of SARS-CoV-2 [13]. $3CL^{pro}$ is a cysteine protease with His41-Cys145 active site, and the substrate-binding site is situated in the cleft between domain I and II, as shown in Fig. 1A [13]. Molecular docking results of standard drug and selected bioactives from HMPs with $3CL^{pro}$ revealed that these bioactives firmly bind at the catalytic dyad of $3CL^{pro}$. Standard drug remdesivir formed four H-bonds with $3CL^{pro}$ residues Leu141, Gly143, His163, and Glu166, furthermore various hydrophobic contacts at the active site (Table 1 and Fig. 1B). Similarly, bioactives from HMPs such as candibirin H formed four H-bonds with $3CL^{pro}$ residues Asn142, Gly143, Cys145, and His163, besides various hydrophobic interactions at the active site (Table 1 and Fig. 1C). Similarly, selected HMP bioactives candibirin G (BE: -9.1 kcal/mol), catechin 5-*O*-gallate (BE: -8.2 kcal/mol), hypericin (BE: -8.8 kcal/mol), and pseudohypericin (BE: -8.5 kcal/mol) have shown a higher binding affinity with the $3CL^{pro}$ and formed strong H-bonding and non-bonded interactions with its active site, as shown in Supplementary Fig. 1. These results suggest that the selected HMP bioactives may likely inhibit the $3CL^{pro}$ activity. The inhibition constant (Ki) calculated for the selected HMP bioactives with $3CL^{pro}$ are summarized in Table 1. The candibirin H bears the lowest Ki value with 180 nM, and the remaining Ki values for the selected HMP bioactives were in the range between 220 and 990 nM.

SARS-CoV-2 PLpro comprises four domains: ubiquitin-like, finger, thumb, and palm domains, as demonstrated in Fig. 2A. There is a high structural similarity between PLpro of SARS-CoV and SARS-CoV-2, and they share an 82.9% sequence identity and a 100% sequence identity for the binding site [33]. The active site of PLpro consists of a catalytic triad of residues Cys111, His272, and Asp286 and is located between the thumb and the palm domains [33–35]. Among the selected HMP bioactives, hypericin had a higher BE of −7.6 kcal/mol than the standard drug remdesivir (−6.2 kcal/mol) (Table 1). Hypericin formed H-bonds with Cys270 and Lys274 of PLpro of SARS-COV-2 and had hydrophobic interactions with Trp106, Gly271, His272, and Asp286 at the active site (Table 1 and Fig. 2C). The interactions of hypericin were similar to the interactions of standard drug remdesivir such as H-bonds with Lys105, His272, and Lys274 as well as hydrophobic interactions with Trp106, Asp286, Ala288, and Leu289 (Table 1 and Fig. 2B). The HMP bioactives, including candibirin H, candibirin G, catechin 5-*O*-gallate, and pseudohypericin were interacting with the catalytic site of PLpro, which are displayed in Table 1 and Supplementary Fig. 2. Ki for selected HMP bioactives was in the range of 2–15 μM, as shown in Table 1.

RdRp is another essential target of SARS-CoV-2 that plays a vital role in the replication and transcription cycle of viruses [36]. RdRp, also called nsp12, in a complex with nsp7 and nsp8, executes the viral genome's replication. The active site of RdRp has remained conserved for many viruses and consists of motifs A-G (Fig. 3A). Motif A consists of residues 611–626, where Asp618 is a critical divalent-cation-binding residue. Ser759, Asp760, and Asp761 are other catalytic residues that are a part of motif C. Nucleotide triphosphate (NTP) entry channel consist of motif F residues Lys545, Arg553, and Arg555 [17]. Our docking analysis of standard drug and HMP bioactives also displayed interaction with residues of the NTP entry channel and active site of RdRp. Standard drug remdesivir interacted with RdRp by forming H-bonds with Arg553, Arg555, Tyr619, Lys621, and Ser682 as well as hydrophobic interactions with Asp623, Asp760, Asp761 as displayed in Table 2 and Fig. 3B. Among HMP bioactives, hypericin (−8.9 kcal/mol) had the highest binding affinity, followed by pseudohypericin (−8.6 kcal/mol), candibirin G (−8.5 kcal/mol), catechin 5-O gallate (−8.0 kcal/mol), and candibirin H (−7.9 kcal/mol) (Table 2). Similarly, hypericin had the lowest Ki (310 nM), and the selected HMP bioactives Ki value ranges from 0.31 μM to 1.65 μM, as shown in Table 2. Hypericin strongly binds at the catalytic site of RdRp by forming H-bonds with Tyr619, Lys621, Cys622, Asp760, and Ser814 as well as hydrophobic interaction with Asp618 (Table 2 and Fig. 3C). Like hypericin and remdesivir, other selected HMP bioactives interact with the NTP entry channel and active site of RdRp (Supplementary Fig. 3).

SARS-CoV-2 helicase forms a triangular-pyramid shape that consists of five domains. These five domains are formed by two RecA-like domains, namely 1A and 2A, present near the core of C terminal helicase, the N-terminal Zinc binding domain (ZBD), the beta-barrel domain (1B), and the stalk domain, which connects 1B and ZBD (Fig. 4A). The helicase enzyme's ATP binding site has hydrolytic activity, which comprises residues Lys288, Ser289, Asp374, Glu375, Gln404, and Arg567, which is present in the cleft between 1A and 2A domain base. This implies that

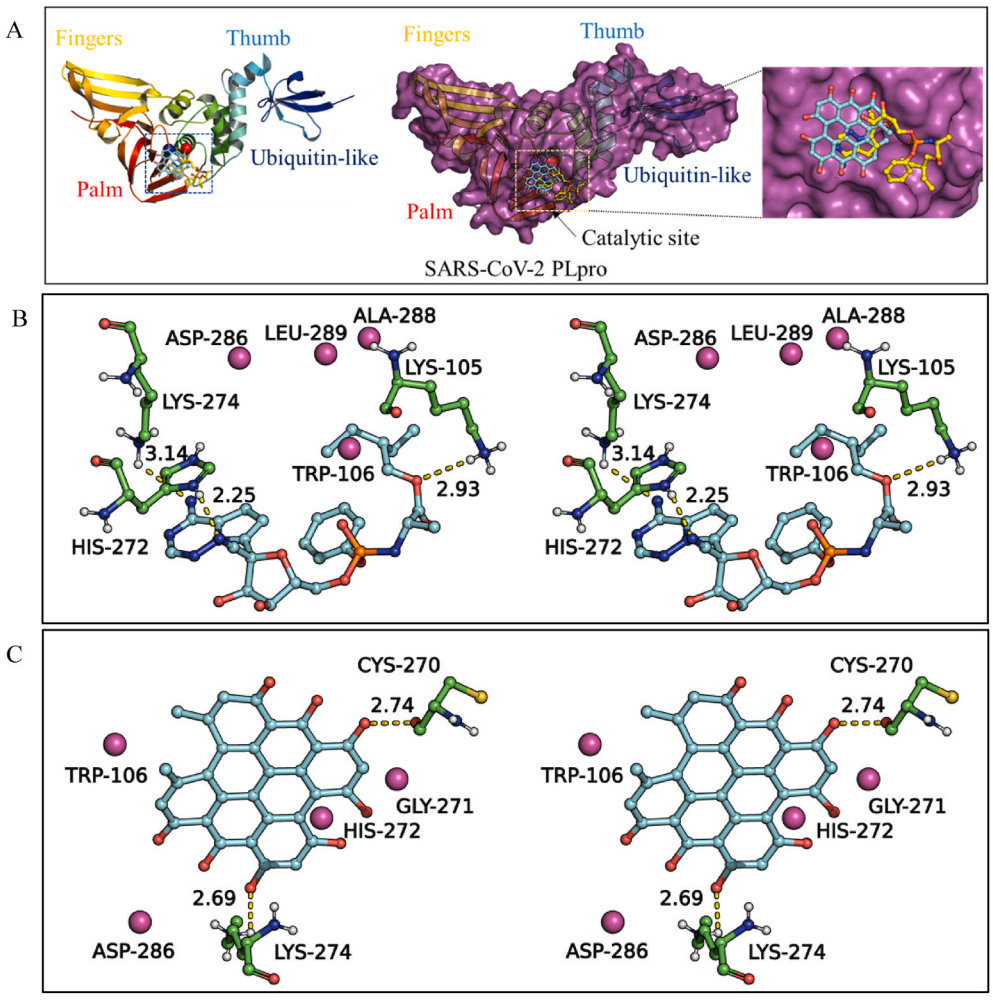

Fig. 2. (A) Secondary structural representation of SARS-CoV-2 PLpro (cartoon and surface representations) consists of four domains viz., ubiquitin-like, finger, thumb, and palm domains. The catalytic site is highlighted in a square box. Remdesivir (yellow) and hypericin (sky blue) at the substrate-binding site are also shown, and its close-up view is displayed in the rightmost panel. (B–C) 3D stereo figures demonstrating molecular interactions of SASR-CoV-2 PLpro (PDB ID: 7JRN) with remdesivir (B) and with bioactive from HMP hypericin (C) are shown. The structural elements of bioactives and their corresponding molecular interactions are shown and colored as represented in Fig. 1.

inhibiting the NTPase activity by blocking the ATP binding site of the enzyme can lead to helicase inhibition [37,38]. Intriguingly, our docking study revealed that the selected HMP bioactives bind at the cleft between 1A and 2A of the enzyme, implying that these bioactives may disrupt ATP binding. Standard drug remdesivir docked at the active site (BE: -8.0 kcal/mol) and formed H-bonds with Gly285, Thr286, Gly287, Lys288, Ser289, His290, and Arg443 as well as several hydrophobic interactions, as given in Table 2 and Fig. 4B. Among HMP bioactives, candibirin H had the lowest BE (−9.1 kcal/mol) and formed three H-bonds with Gly285, Ala312, and Ala316 (Table 2 and Fig. 4C).

Table 2
Binding energies (BEs) (kcal/mol) of selected bioactives from the Himalayan medicinal plants against SARS-CoV-2 RdRp and helicase along with their hydrogen bonding (H-bond), hydrophobic interactions (HP), and inhibition constant (Ki) are shown. The bioactive compounds' names are displayed in **boldface**, and the plant names are given in *italics*.

Himalayan medicinal plants and their bioactives	SARS-CoV-2 RdRp				SARS-CoV-2 Helicase			
	BE	H-Bond	HP	Ki (μM)	BE	H-Bond	HP	Ki (μM)
Remdesivir*	−7.1	Arg553, Arg555, Tyr619, Lys621, Ser682	Asp623, Asp760, Asp761	6.34	−8.0	Gly285, Thr286, Gly287, Lys288, Ser289, His290, Arg443	Glu319, Lys320, Asp374, Glu375, Glu540	1.39
Candibirin H *Heracleum candicans* Wall.	−7.9	Arg553, Arg555, Ser814	Arg555, Asp618, Tyr619, Asp623, Ser759, Cys813	1.65	−9.1	Gly285, Ala312, Ala316	Pro284, Lys288, Asp315, Glu375, Arg443, Glu540	0.22
Candibirin G *Heracleum candicans* Wall.	−8.5	Arg553, Thr556, Asn691, Asp760	Tyr455, Lys545, Lys621, Asp623	0.60	−8.9	Gly285, Ser289	Lys288, Ala316, Glu319, Arg443	0.31
Catechin 5-O-gallate *Acacia nilotica*	−8.0	Arg553, Tyr619, Asp760, Glu811, Cys813, Ser814	Asp618, Lys621, Asp623, Trp800	1.39	−8.7	Gly285, Lys288, Gln404, Gln537, Gly538, Glu540, Arg567	Arg442, Arg443	0.43
Hypericin *Hypericum perforatum* L.	−8.9	Tyr619, Lys621, Cys622, Asp760, Ser814	Asp618	0.31	−8.0	–	Lys288, Ser289, Ala312, Ala313, Ala316, Gln537, Asp374	1.39
Pseudohypericin *Hypericum perforatum* L.	−8.6	Lys621, Cys622, Asp760, Ser814	Asp618, Lys798	0.51	−8.0	Ser289, Ser310	Lys288, Ala312, Ala313, Ala316, Glu375	1.39

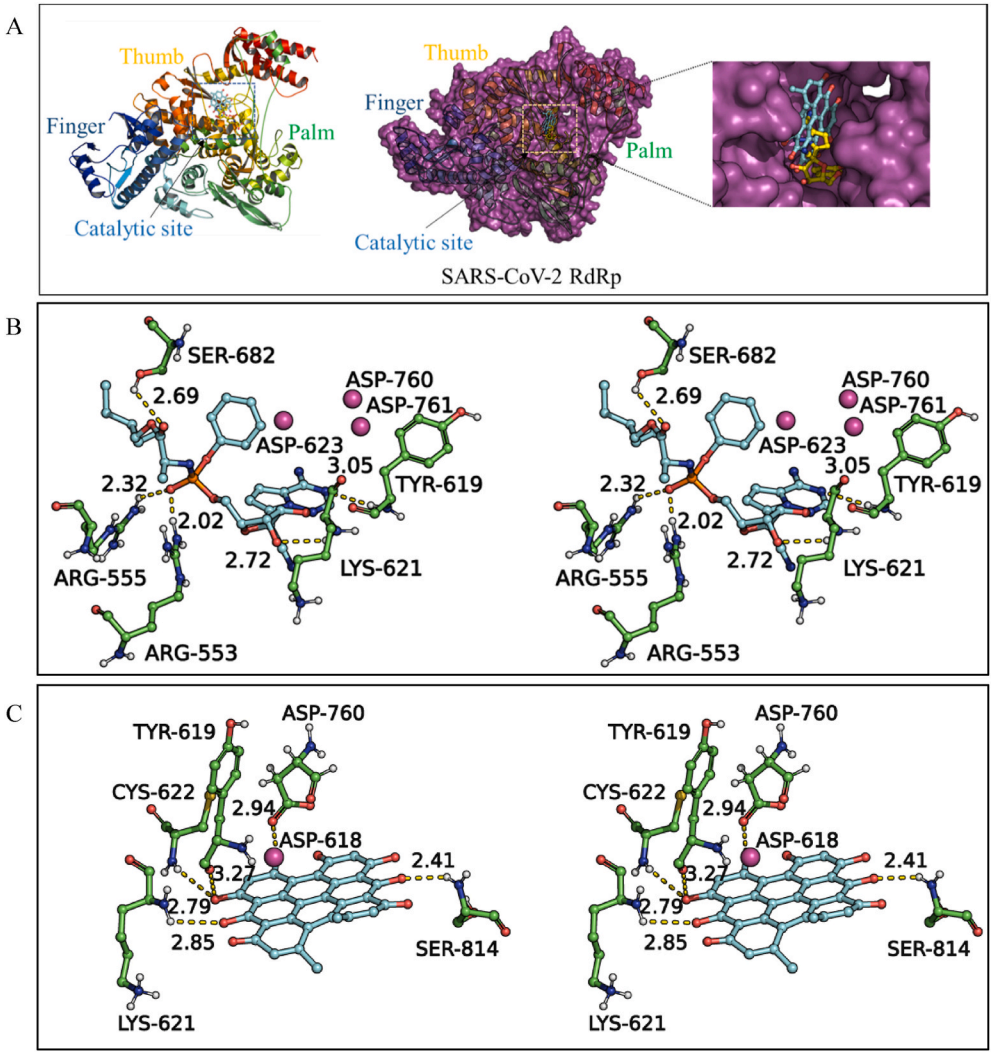

Fig. 3. (A) Secondary structural representation of SARS-CoV-2 RdRp (cartoon and surface representations) consists of domains viz., finger, thumb, and palm domains. The catalytic site is highlighted in a square box. Remdesivir (yellow) and hypericin (sky blue) at the substrate-binding site are also shown with its close-up view (rightmost panel). (B–C) 3D stereo figures demonstrating molecular interactions of SASR-CoV-2 RdRp (PDB ID: 6M71) with Remdesivir (B) and with the bioactive from HMP, hypericin (C) are shown. The structural elements of bioactives and their corresponding molecular interactions are displayed and colored, as in Fig. 1.

Similarly, HMP bioactives like candibirin G (−8.9 kcal/mol), catechin 5-*O*-gallate (−8.7 kcal/mol), hypericin (−8.0 kcal/mol), and pseudohypericin (−8.0 kcal/mol) had lower binding energies and interacted at the catalytic site as displayed in Table 2 and Supplementary Fig. 4. Likewise, lower Ki was found for the selected HMP bioactives with SARS-CoV-2 helicase ranging between 0.22 and 1.39 μM as given in Table 2.

3.1.2. *HMP bioactives with SARS-CoV-2 transmission targets*

SARS-CoV-2 spike protein is made up of S1 and S2 domains. The S1 domain forms the receptor-binding domain (RBD) (Fig. 5A), whereas the S2 domain forms the membrane fusion protein. The RBD of spike protein recognizes and binds to the human ACE2 receptor of the host cell and thus infecting the host cell. Molecular analysis of spike protein receptor-binding motif (RBM) and human ACE2 complex revealed different spike protein residues, and hotspot residues of the ACE2 receptor are involved in the virus's interaction with the host cell. The ACE2 receptor comprises two viral-binding hotspots: Lys31 (hotspot 31) and, Lys353 (hotspot 353) (Fig. 6A). Hotspot 31 includes a salt bridge between Lys31 and Glu35, and hotspot 353 composed of a salt bridge between Lys353 and Asp38 covered in a hydrophobic environment. The spike protein's vital amino acid residues include Leu455, Phe486, Gln493, and Ser494, which bind to the ACE2 receptor [3–5,14].

To understand the potential capability of HMP bioactives against transmission targets SARS-CoV-2 spike protein and human ACE2 receptor, molecular docking analysis were carried out along with the standard drugs. Similar to the replication targets, among the standard drugs remdesivir also had a superior binding affinity and bound with spike protein and ACE2 receptor having a BE of −6.6 kcal/mol and −6.4 kcal/mol, respectively (Supplementary Table S3). Among HMP bioactives, hypericin had the highest binding affinity with spike protein (−8.3 kcal/mol), and tribuloside had a higher binding affinity with ACE2 (−7.4 kcal/mol). Based on the BEs of standard drug and HMP bioactives, we set the cut-off BE of −7.0 kcal/mol, and −6.5 kcal/mol for spike protein and ACE2, respectively. These cut-off binding energies were used to select the superior HMP bioactives as described in section 3.1.1. Based on the cut-off binding energies, six bioactives from HMP bioactives were selected for protein-ligand interaction studies and biological pathway enrichment analysis. The selected HMP bioactives were 6,6′-biapigenin, hypericin, kaempferol 3-glucoside 7-rhamnoside, kaempferol 7,4′-diglucoside, tribuloside, and tribulosin and their BE, as well as interactions, are summarized in Table 3.

Standard drug remdesivir (BE: -6.6 kcal/mol) formed five H-bonds at the spike protein receptor-binding motif, including Arg403, Tyr453, Gln493, Gly496, and Asn501, as well as hydrophobic interactions with Leu455, Phe456, and Tyr489 (Table 3 and Fig. 5B). Firm binding and impeding interaction between spike protein receptor-binding motif and ACE2 receptor provide a crucial opportunity to hinder the transmission of SARS-CoV-2. In line with this, HMP bioactives were also found to bind at the receptor-binding motif of spike protein firmly. For example,

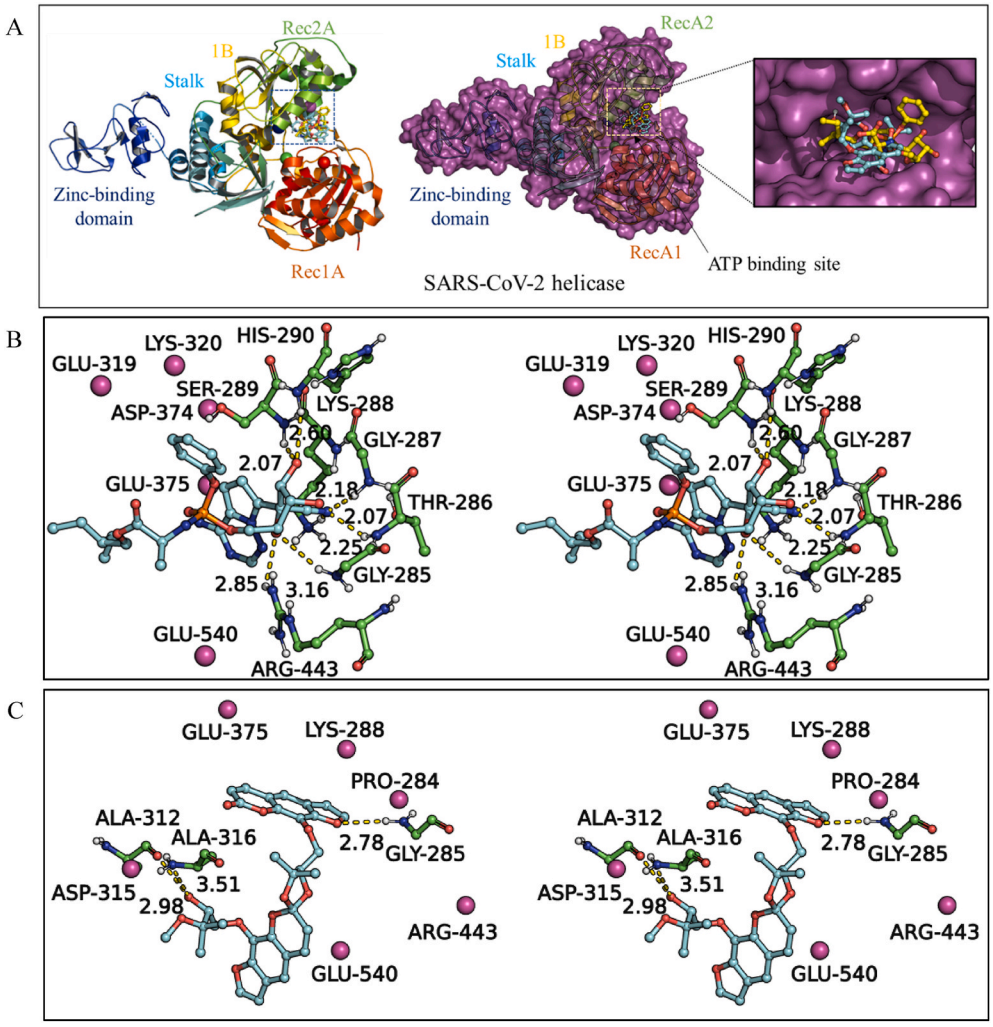

Fig. 4. (A) Secondary structural representation of SARS-CoV-2 helicase (cartoon and surface representation) consists of five domains viz., RecA-like domains, namely 1A and 2A, zinc-binding domain (ZBD), the beta-barrel domain (1B), and the stalk domain. ATP-binding site is highlighted in a square box. The remdesivir (yellow) and candibirin H (sky blue) at the ATP-binding site are also displayed in the square box with its close-up view (rightmost panel). (B–C) 3D stereo figures demonstrating molecular interactions of SASR-CoV-2 helicase (PDB ID: 6ZSL) with remdesivir (B) and with the bioactive from HMP, candibirin H (C) are shown. The structural elements of bioactives and their corresponding molecular interactions are represented and colored as in Fig. 1.

Table 3
Binding energies (BEs) (kcal/mol) of selected bioactives from the Himalayan medicinal plants against SARS-CoV-2 spike protein and human ACE2, along with their hydrogen bonding (H-bond), hydrophobic interactions (HP), and inhibition constant (Ki), are shown. The bioactive compounds' names are displayed in **boldface**, and the plant names are given in *italics*.

Himalayan medicinal plants and their bioactives	SARS-CoV-2 Spike protein				Human ACE2			
	BE	H-Bond	HP	Ki (μM)	BE	H-Bond	HP	Ki (μM)
Remdesivir	−6.6	Arg403, Tyr453, Gln493, Gly496, Asn501	Leu455, Phe456, Tyr489	14.74	−6.4	His34	Asn33, His34, Glu37, Asp38, Tyr41,Lys353	20.64
6,6′-biapigenin *Hypericum perforatum* L.	−7.9	Glu484, Phe490, Leu492, Ser494	Leu452, Phe486, Tyr489	1.65	−6.6	His34, Asp38	Phe28, Lys31, Tyr41	14.74
Hypericin *Hypericum perforatum* L.	−8.3	Ser494	Tyr449, Leu452, Leu492, Gln493	0.84	−6.7	Glu75, Gln76	Phe28, Lys31, Leu79, Tyr83	12.45
Kaempferol 3-glucoside 7-rhamnoside *Acacia nilotica*	−7.1	Arg403, Glu406, Gln409, Tyr449, Gln493	Tyr449, Tyr505	6.34	−6.5	Asn33, Phe390, Arg393	Glu37, Asp38, Lys353	17.44
Kaempferol7,4′-diglucoside *Acacia nilotica*	−7.3	Arg403, Gly485, Cys488, Phe490, Gln493, Ser494, Gly496	Tyr453, Leu455, Phe456, Tyr495, Tyr505	4.53	−8.1	Lys26, Leu29, Asp38, Gln96, Gln388, Arg393	Asp30, Asn33, Glu37, Lys35, Pro389	1.18
Tribuloside *Tribulus terrestris* L	−8.0	Arg403, Gln409, Tyr453, Gln493	Lys417, Tyr453, Leu455, Gln493, Tyr495, Tyr505	1.39	−7.4	Glu37, Asp38, Gln96, Arg393	Asn33, Glu37, Asp38, Lys353	3.83
Tribulosin *Tribulus terrestris* L.	−7.7	Tyr453, Phe490, Leu492, Gln493, Ser494, Gly496	–	2.31	−6.6	Asp30, Lys31, His34, Glu35	Asp38	14.74

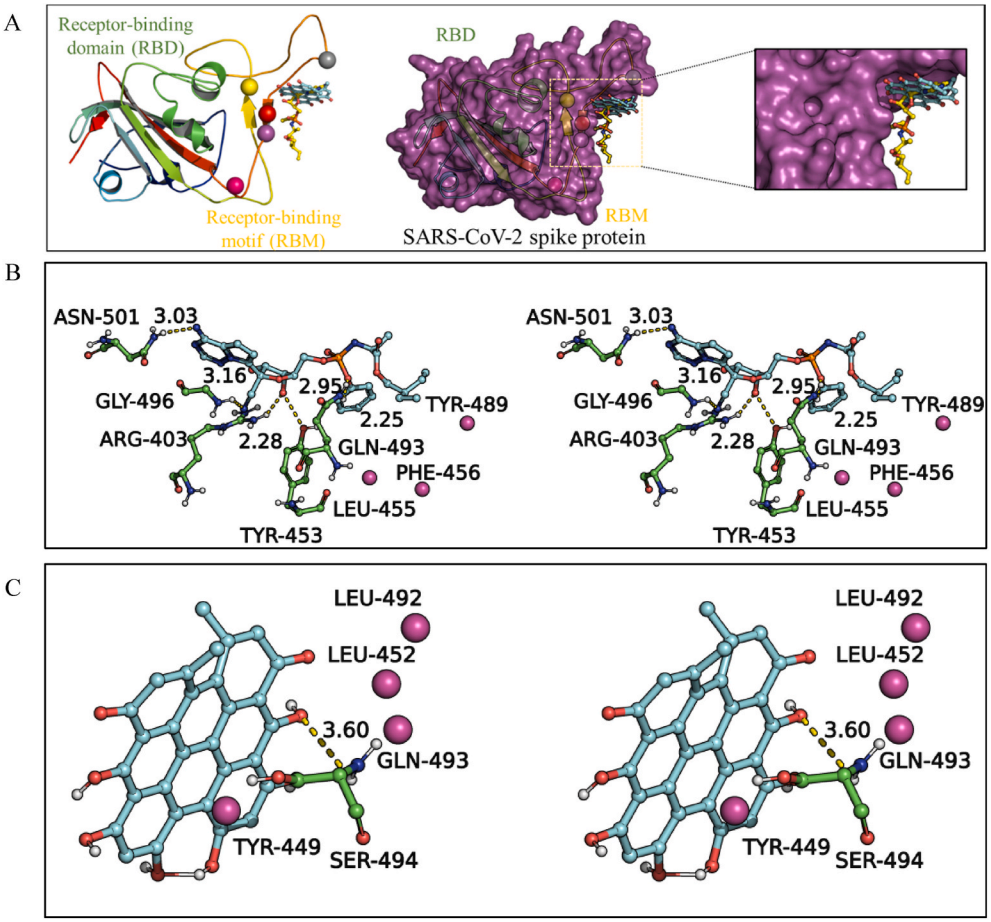

Fig. 5. (A) Secondary structural representation of SARS-CoV-2 spike protein (cartoon and surface representation) containing spike protein receptor-binding motif. The receptor-binding motif is represented as spheres (spheres represent different critical residues of receptor-binding motif yellow: Leu455, red: Gln493, pink: Asp501, purple: Ser494, and grey: Phe486). The docked molecules remdesivir (yellow) and hypericin (sky blue) at the receptor-binding motif are also shown with its close-up view (rightmost panel). (B–C) 3D stereo figures demonstrating molecular interactions of SASR-CoV-2 spike protein (PDB ID: 6W41) with remdesivir (B) and with the bioactive from HMP, hypericin (C) is displayed. The structural elements of bioactives and their corresponding molecular interactions are represented and colored as in Fig. 1.

hypericin makes H-bonding with Ser494 and hydrophobic interactions with Tyr449, Leu452, Leu492, and Gln493 residues of spike protein RBM (Table 3 and Fig. 5C). Similar to the hypericin, other selected HMP bioactives also strongly interact with spike protein RBM (Table 3, Supplementary Fig. 5).

Besides, HMP bioactives also had strong interactions with hotspot residues of the ACE2 receptor. Bioactives 6,6′-biapigenin, hypericin, and tribulosin had interaction with residues of hotspot Lys31 of ACE2 receptor. Bioactives kaempferol 3-glucoside 7-rhamnoside, kaempferol 7,4′-diglucoside, and tribuloside interact with residues hotspot Lys353 of ACE2 (Table 3, Fig. 6 and Supplementary Fig. S6), and the interactions of remdesivir and kaempferol 7,4′-diglucoside with ACE2 receptor are displayed in Fig. 6B and C. The Ki was also calculated for the selected HMP bioactives with spike protein and ACE2 and are summarized in Table 3. Ki for the selected HMP bioactives with spike protein and ACE2 were found to be less than 40 μM stating that the selected HMP bioactives have a significant binding affinity with these target proteins. On the other hand, targeting ACE2 may have several biological consequences, such as functional deterioration of the heart and progression of cardiac, renal, and vascular pathologies. However, elevated levels of the catalytic active ACE2 were found in the SARS-CoV-2 infected patients [39]. This might be due to the infiltration of immune cells such as macrophages and neutrophils, which overexpressed the ACE2 during the infection. Therefore, like other diseases, the dose of the HMP bioactives needs to be adjusted to effectively reduce the elevated expression of ACE2 into the basal level. Further, the interaction of the SARS-CoV-2 spike protein receptor-binding motif with hotspot residues of ACE2 differs from the active site of ACE2. Spike protein receptor-binding motif interacts with hotspot residues Lys353 and Lys31 with S1 subunit. Hence, targeting the ACE2 receptor holds an advantage in the attenuation of spike protein interaction and attachment.

Overall, among HMP bioactives, hypericin from *H. perforatum* has shown its potential in targeting all the six proteins involved in the replication and transmission of COVID-19. The presence of hypericin makes *H. perforatum* a primary photosensitizer. In clinical trials, hypericin appeared in the blood after a single oral administration of *H. perforatum* extract. Furthermore, the steady-state level of hypericin in the blood has been observed after long-term dosing. The polyphenol fraction of *H. perforatum* has shown immune-stimulating activity, whereas the lipophilic portion has shown immunosuppressing properties. Moreover, in acute toxicity studies, the extract has led to a relatively nontoxic effect in rats, guinea pigs, and mice [40]. Besides, the extract and the oil of this plant are used widely in a range of products. For example, *H. perforatum* extract is used in more than 50 cosmetic formulations, and the oil in more than ten products. Therefore, this extract with other combinations of HMP bioactives may likely be used to make formulations to inhibit COVID-19 infection and transmission.

However, the dire situation of SARS-CoV-2 has been further escalated due to the emergence of highly fit SARS-CoV-2 variants [41]. Currently, various strains of SARS-CoV-2 with several mutations of its proteins have been reported. For example, one of the mutations, R408I, in the spike protein happens to lie in the receptor-binding domain. This mutation has been reported to increase the stability of the spike protein [42]. Also, R60C mutation in the $3CL^{pro}$ was observed to have an impact on the root mean square fluctuation (RMSF) of the protein structure. Further, MD simulation results revealed that the ligand-binding affinity to the mutated $3CL^{pro}$ was decreased compared to the wild type $3CL^{pro}$ [42]. In another study, D614G mutation in the spike protein and P323L mutation in the RdRp protein has been reported to have a high incidence of 43.27% and 43.21%, respectively. These mutations were not reported

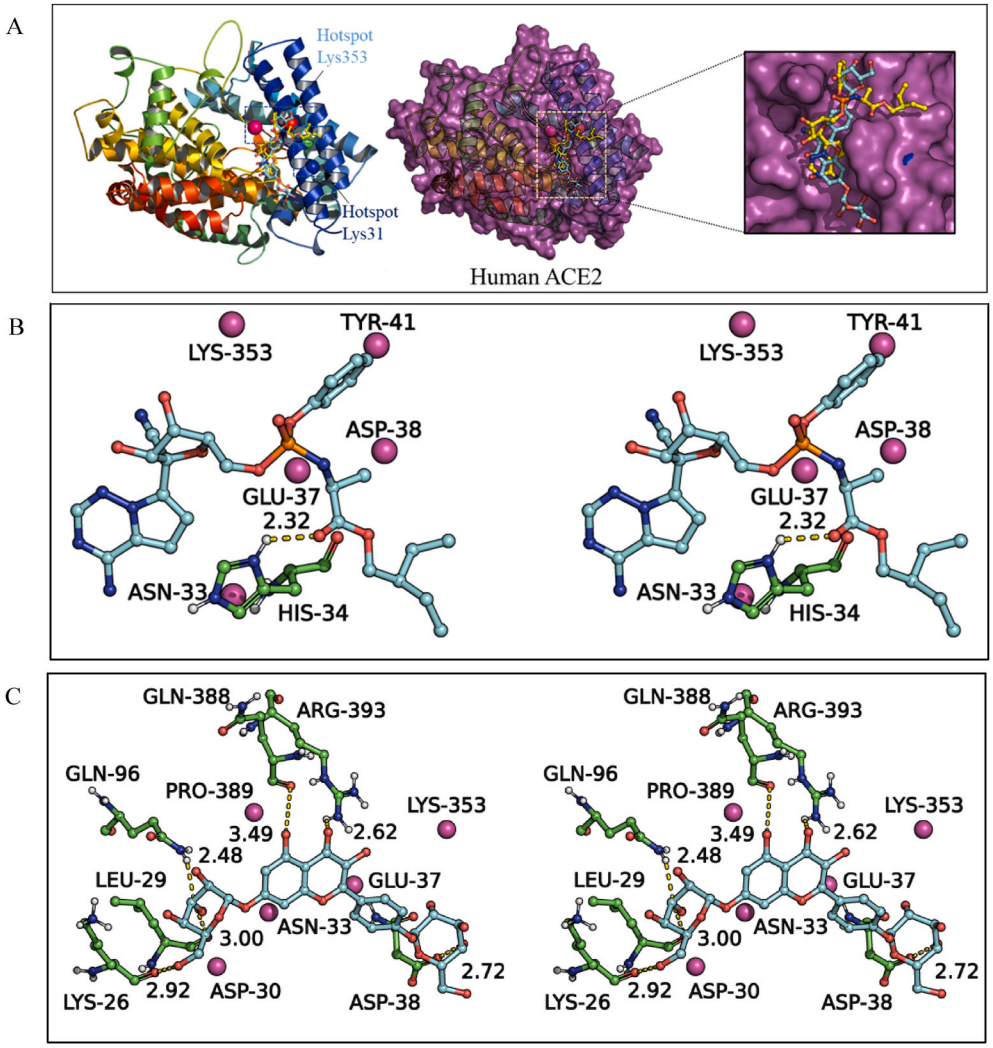

Fig. 6. (A) Secondary structural representation of human ACE2 (cartoon and surface representation) representing hotspot spike-protein binding regions. Viral-binding hotspots are defined in a square box. The molecules remdesivir (yellow) and kaempferol 7,4′-diglucoside (sky blue) docked near the hotspot residues also highlighted in the square box with its close up view (rightmost panel). (B–C) 3D stereo figures demonstrating molecular interactions of human ACE2 (PDB ID: 1R42) with remdesivir (B) and with the bioactive from HMP, kaempferol 7, 4′-diglucoside (C) are displayed. The structural elements of bioactives and their corresponding molecular interactions are represented and colored as in Fig. 1.

to have a significant change in the protein structure. However, D614G mutation in the spike protein has been observed to cause an increase in viral infection. Mutations Q57H and G251V in the ORF3a protein and mutations S194L and R203K/G204R in the nucleocapsid protein were observed to cause a structural change in the respective proteins [43]. These reports indicate mutations in the SARS-CoV-2 proteins may reduce the binding efficiency of HMP bioactives. Thus, to overcome the limitations of SARS-CoV-2 mutations, we have identified HMP bioactives that can target multiple protein targets. Hence, apart from the mutated proteins, HMP bioactives can also bind with other target proteins and may likely attenuate the life cycle of SARS-CoV-2.

3.2. *Biological pathway enrichment analysis of the human protein targets distinguished for the HMP bioactives and SARS-CoV-2*

Top fifteen human protein targets were obtained for each of the bioactives from SwissTargetPrediction, listed in Supplementary Table S4. Human protein targets for SARS-CoV-2 were obtained from the literature survey, also summarized in Supplementary Table S4. Pathway enrichment analysis was performed for both the HMP bioactive targets and the SARS-CoV-2 targets using the Enrichr.

It was observed that viral infection pathways, immunity, and apoptosis were common for both bioactives and SARS-CoV-2 targets. Enrichr was used to perform gene ontology (GO) enrichment of biological processes concerning *p*-values obtained by Fisher exact test for bioactives and SARS-CoV-2. Further, after redundancy removal using Revigo, scatterplot revealed distinct clusters of GO terms of biological processes for HMP bioactive targets and SARS-CoV-2 targets (Fig. 7). Each cluster represents semantically similar GO terms. Regulation of protein kinase B signaling (PKB/Akt) and cytokine-mediated signaling pathways were the most enriched term among biological pathways for the HMP bioactives and SARS-CoV-2, respectively (Fig. 7). Biological process enrichment analysis revealed that bioactives and SARS-CoV-2 targets commonly regulate the cytokine and apoptosis signaling pathways. MAPK pathway, shown to be targeted by the bioactives, is activated upon external stress.

When SARS-CoV-2 infects a host cell, spike protein binds to ACE2, thus downregulating its expression. As a result, p38 MAPK is highly upregulated, which causes a cytokine storm (IL-6, TNF-α, and IL-1β), leading to inflammation [44].

Further, the bioactives target the PKB/Akt, which is involved in metabolism, cell proliferation, and cell survival. 3-phosphoinositide-dependent protein kinase-1 (PDK1) helps to regulate the PKB/Akt pathway. Upon infection by SARS-CoV, $3CL^{pro}$ interacts with PDK1, thereby hindering its interaction with PKB/Akt. This lowers PKB/Akt phosphorylation. As a result, apoptosis is induced in the viral affected cells [45]. Therefore, it may be assumed that bioactives targeting these pathways might help control SARS-CoV-2 infection. Another pathway targeted by bioactives in the calcium-mediated pathways. Viruses are known to disrupt calcium homeostasis, thus altering the membrane permeability and promoting viral infection into the cell [46]. Hence, bioactives might likely be used to target the calcium-mediated pathways

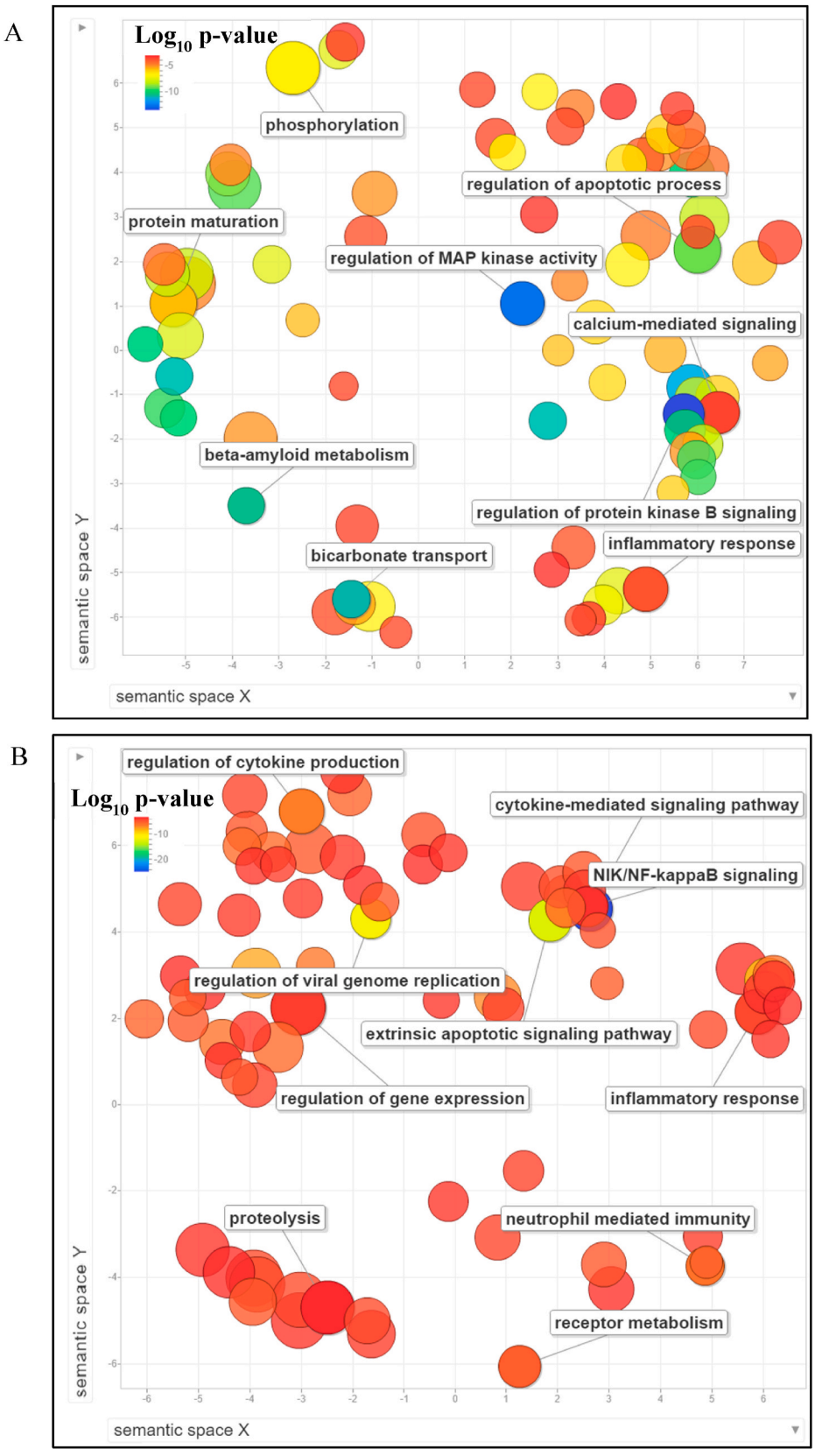

Fig. 7. Scatterplot showing clusters of GO biological processes enrichment analysis. (A) HMP bioactives. (B) SARS-CoV-2. The scatterplot shows clusters of GO terms after redundancy removal. Bubble size represents the frequency of the GO term in the GO database. The color of the bubbles represents the Log_{10} *p*-values (a legend in the upper left-hand corner).

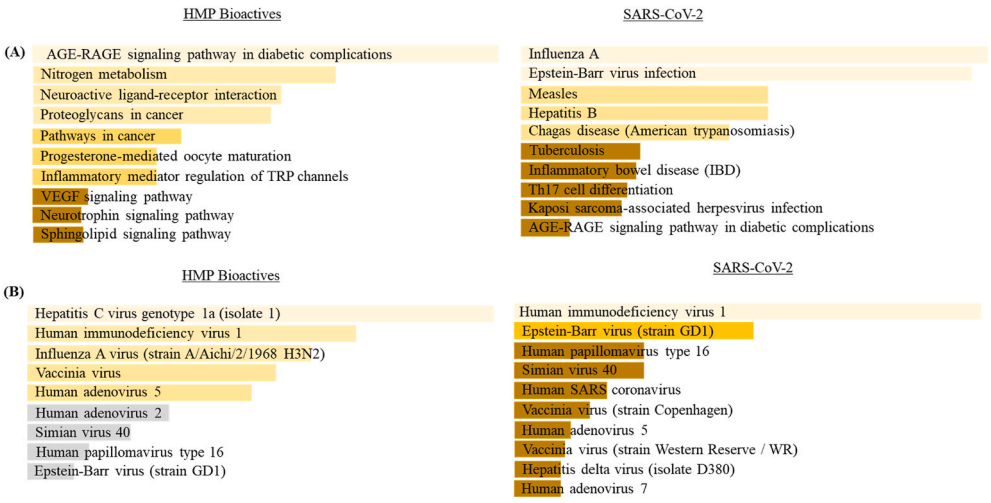

Fig. 8. Top 10 enrichment analyses of (A) KEGG Pathway and (B) VirusMINT database for the identified HMP bioactive targets and SARS-CoV-2 targets. The bars represent *p*-values that are calculated using the Fisher Exact Test. The longer and lighter the bar color, the more significant is the respective biological activity.

to disrupt the entry of the viral genome.

Enrichr results for KEGG pathway enrichment analysis showed that the AGE-RAGE signaling pathway in diabetic complications and nitrogen metabolism was most enriched for bioactives. Influenza A and Epstein-Barr virus infection were most enriched for SARS-CoV-2 (Fig. 8A). Advanced glycation end products (AGEs) are present in higher levels in diabetic patients. SARS-CoV-2 infection increases COVID-19 severity and also the risk of mortality in diabetic patients [47]. Furthermore, tryptophan metabolism was found to be highly affected in COVID-19 patients. Tryptophan levels were highly reduced and found to be inversely related to IL-6 levels, suggesting renal dysfunction [48]. Hence, implying that these bioactives may help control the risk of mortality in patients who have COVID-19 along with comorbidities such as diabetes and renal dysfunction. KEGG enrichment analysis for SARS-CoV-2 targets revealed a pathway associated with Influenza A as both lead to respiratory distress.

Through VirusMINT database enrichment analysis, it was observed that the targets of both the HMP bioactives and SARS-CoV-2 are also targeted by Human Immunodeficiency Virus 1 (Fig. 8B). Additionally, human protein targets of Hepatitis C and Influenza A were also observed for the bioactive targets. Anti-viral drugs used in the treatment of these diseases are being used against SARS-CoV-2 [49]. This further proposes that the selected HMP bioactives can likely be used against SARS-CoV-2 and control other viral RNA infections.

3.3. ADME/T evaluation of HMP bioactives

ADME/T estimation is used to predict the pharmacological parameters such as absorption, distribution, metabolism, excretion, and toxicity of a compound. After human intestinal absorption (HIA), compounds reach into circulation. Caco-2 permeability mimics the HIA *in vitro* system. Hence, we have evaluated the ADME/T properties of selected HMP bioactives and are represented in Table 4. We have found that among selected HMP bioactives, candibirin G, candibirin H, and hypericin have shown optimal Caco-2 permeability and human intestinal absorption. Also, all the selected bioactives function as P-glycoprotein (P-gp)-inhibitor; however, none of them function as P-gp-substrate. Therefore, the retention time of bioactives inside the cells will be enhanced, which may promote the activity of the bioactives. After absorption, these selected bioactives have shown a lesser binding affinity towards plasma protein (PPB); consequently, the bioavailability of these bioactives may enhanced. After distribution to the different organs, bioactives are metabolized in the liver by different metabolic enzymes, especially cytochrome P450 enzymes [50]. We have found here that some of the bioactives function as CYP450 enzyme substrates, which are metabolized quickly through these enzymes. In contrast, some bioactives have CYP450 enzyme inhibitory potential, which hinders the metabolism. The half-life of these selected HMP bioactives is low except for hypericin. Besides, we have not found any adverse toxicity of the selected HMP bioactives *in silico*. None of the selected bioactive compounds have shown hepatotoxicity, though candibirin G and candibirin H have shown minimal hepatotoxicity. Most of the selected bioactives function as moderate hERG blockers. Moderate hERG blockade may produce a beneficial class III antiarrhythmic effect [51].

3.4. Predicted biological activities of HMP bioactives

Several possible biological activities of the selected HMP bioactives were predicted using the prediction of activity spectra for substances (PASS) webserver. Two factors evaluate biologically active compounds; Pa signifies the probability “to be active”, and Pi signifies the probability “to be inactive”. The value of both factors ranging from 0 to 1. Here, we found most of the bioactives function as potent membrane integrity agonists and membrane permeability inhibitors. Besides, they also have anti-inflammatory, antitussive, and anti-viral activities, especially against the influenza virus. Among them, tribulosin may likely function as respiratory analeptic to recover from respiratory depression. Intriguingly, several HMP bioactives have shown anti-viral activity against several genera of viruses, as shown in Table 5. These results suggest that HMP bioactives have pleiotropic biological activities that can enhance the therapeutic application against COVID-19.

4. Conclusion

The unending COVID-19 pandemic has increased morbidity and mortality across the globe. Our study revealed that the selected HMP bioactives formed stable interactions with SARS-CoV-2 target proteins involved in viral infection and replication. The selected HMP bioactives were found to bind with a higher affinity at the active sites of replication target proteins and receptor-binding motif as well as hotspot residues of the transmission targets. Among them, hypericin from *H. perforatum* is the most potent compound, which actively targets all six proteins involved in replicating and transmitting COVID-19. Numerous literature has also shown the health beneficiary role of hypericin, and currently, several hypericin-based products are available in the market. Therefore, the hypericin extract can be used in several phyto/food formulations with other selected potential HMP bioactives to treat the COVID-19. The Ki values of the selected HMP bioactives were also lower than 40 μM

Table 4
ADME/T prediction of selected bioactives from HMP

Class	Properties	6,6' Biapigenin	Candibirin G	Candibirin H	Catechin 5-O-gallate	Hypericin
Absorption	Caco-2 permeability (> -5.15 cm/s)	Not optimal -6.351 cm/s	Optimal -5.06 cm/s	Optimal -5.06 cm/s	Not optimal -6.716 cm/s	Not optimal -6.277 cm/s
	Pgp-inhibitor	+ 0.649	++ 0.863	++ 0.863	++ 0.727	— 0.04
	Pgp-substrate	— 0.022	— 0.166	— 0.166	— 0.044	— 0.071
	HIA (Human Intestinal Absorption) (≥30%: HIA+; <30%: HIA-)	- 0.43	+ 0.5	+ 0.5	- 0.355	- 0.499
	F (20% Bioavailability) (≥20%: F20+; <20%: F20-)	+ 0.572	- 0.434	- 0.434	+ 0.522	+ 0.616
Distribution	PPB (Plasma Protein Binding) (90%)	83.574 %	82.842 %	82.842 %	86.718 %	79.862 %
	Volume distribution (0.04~20 L/kg)	-0.821 L/kg	-0.169 L/kg	-0.169 L/kg	-1.187 L/kg	-1.026 L/kg
	BBB (Blood–Brain Barrier) (BB ratio >=0.1: BBB+; BB ratio <0.1: BBB-)	— 0.236	- 0.38	- 0.38	++ 0.736	++ 0.885
Metabolism	P450 CYP1A2 inhibitor	++ 0.812	— 0.15	— 0.15	— 0.099	++ 0.848
	P450 CYP1A2 substrate	- 0.428	- 0.488	- 0.488	- 0.424	- 0.444
	P450 CYP3A4 inhibitor	++ 0.827	++ 0.847	++ 0.847	- 0.312	— 0.042
	P450 CYP3A4 substrate	- 0.458	+ 0.674	+ 0.674	+ 0.532	- 0.336
	P450 CYP2C9 inhibitor	— 0.156	+ 0.517	+ 0.517	— 0.251	— 0.116
	P450 CYP2C9 substrate	+ 0.619	- 0.352	- 0.352	- 0.488	- 0.398
	P450 CYP2C19 inhibitor	— 0.116	— 0.2	— 0.2	+ 0.568	— 0.119
	P450 CYP2C19 substrate	- 0.403	- 0.469	- 0.469	- 0.404	- 0.496
	P450 CYP2D6 inhibitor	- 0.455	+ 0.513	+ 0.513	- 0.404	— 0.235
	P450 CYP2D6 substrate	- 0.484	- 0.425	- 0.425	+ 0.517	- 0.322
Excretion	$T_{1/2}$ (Half Life Time) (>8h: high; 3h< Cl < 8h: moderate; <3h: low)	Low 2.432 h	Low 2.044 h	Low 2.044 h	Low 1.494 h	Moderate 3.306 h
	Clearance rate (>15 mL/min/kg:high; 5mL/min/kg< Cl < 15mL/min/kg: moderate; <5 mL/min/kg: low)	Low 1.177 mL/min/kg	Low 1.103 mL/min/kg	Low 1.103 mL/min/kg	Low 1.201 mL/min/kg	Low 0.671 mL/min/kg
Toxicity	hERG (hERG Blockers)	+ 0.666	++ 0.722	++ 0.722	+ 0.662	- 0.494
	H-HT (Human Hepatotoxicity)	— 0.248	+ 0.528	+ 0.528	- 0.366	— 0.182
	Ames (Ames Mutagenicity)	- 0.388	— 0.298	— 0.298	- 0.47	— 0.292
	Skin sensitization	— 0.282	— 0.263	— 0.263	— 0.271	- 0.313
	FDAMDD (Maximum Recommended Daily Dose	+ 0.608	— 0.272	— 0.272	+ 0.624	+ 0.674

Class	Properties	Pseudohypericin	Kaempferol 3-glucoside 7-rhamnoside	Kaempferol 7,4 diglucoside	Tribuloside	Tribulosin
Absorption	Caco-2 permeability (> -5.15 cm/s)	Not optimal -6.466 cm/s	Not optimal -6.485 cm/s	Not optimal -6.651 cm/s	Not optimal -6.433 cm/s	Not optimal -6.417 cm/s
	Pgp-inhibitor	— 0.06	- 0.401	- 0.393	++ 0.723	++ 0.802
	Pgp-substrate	— 0.101	— 0.053	— 0.011	— 0.039	— 0.082
	HIA (Human Intestinal Absorption) (≥30%: HIA+; <30%: HIA-)	- 0.427	— 0.184	— 0.107	— 0.127	— 0.162
	F (20% Bioavailability)	+ 0.559	+ 0.56	- 0.451	- 0.443	— 0.26
Distribution	PPB (Plasma Protein Binding) (90%)	80.653 %	75.785 %	75.492 %	85.891 %	50.279 %
	Volume distribution (0.04~20 L/kg)	-0.719 L/kg	-1.06 L/kg	-1.092 L/kg	-0.733 L/kg	-0.574 L/kg
	BBB (Blood–Brain Barrier) (BB ratio>=0.1: BBB+; BB ratio <0.1: BBB-)	++ 0.709	— 0.015	— 0.098	— 0.04	— 0.162
Metabolism	P450 CYP1A2 inhibitor	+ 0.657	— 0.158	— 0.127	— 0.288	— 0.061

(*continued on next page*)

Table 4 (*continued*)

Class	Properties	Pseudohypericin	Kaempferol 3-glucoside 7-rhamnoside	Kaempferol 7,4 diglucoside	Tribuloside	Tribulosin
	P450 CYP1A2 substrate	-	—	—	—	—
		0.438	0.228	0.178	0.257	0.266
	P450 CYP3A4 inhibitor	—	—	—	+	+
		0.11	0.151	0.072	0.615	0.509
	P450 CYP3A4 substrate	-	-	-	-	-
		0.44	0.366	0.31	0.372	0.495
	P450 CYP2C9 inhibitor	—	—	—	-	-
		0.131	0.158	0.109	0.398	0.431
	P450 CYP2C9 substrate	-	-	-	-	—
		0.361	0.366	0.481	0.469	0.218
	P450 CYP2C19 inhibitor	—	—	—	—	—
		0.09	0.07	0.075	0.268	0.088
	P450 CYP2C19 substrate	+	-	-	-	-
		0.51	0.405	0.35	0.322	0.378
	P450 CYP2D6 inhibitor	-	-	-	-	-
		0.332	0.351	0.323	0.406	0.334
	P450 CYP2D6 substrate	-	—	-	-	—
		0.333	0.276	0.305	0.345	0.275
Excretion	$T_{1/2}$ (Half Life Time)	Moderate	Low	Low	Low	Low
	(>8h: high;	3.042 h	2.09 h	2.194 h	2.299 h	2.70 h
	3h< Cl < 8h: moderate;					
	<3h: low)					
	Clearance rate (>15 mL/min/kg:high; 5mL/min/	Low	Low	Low	Low	Low
	kg< Cl < 15mL/min/kg: moderate;	0.212 mL/min/	0.701 mL/min/kg	0.656 mL/min/kg	0.998 mL/	0.189 mL/
	<5 mL/min/kg: low)	kg			min/kg	min/kg
Toxicity	hERG (hERG Blockers)	+	+	+	+	+
		0.511	0.582	0.648	0.672	0.664
	H-HT (Human Hepatotoxicity)	—	—	—	-	—
		0.072	0.212	0.17	0.314	0.0
	Ames (Ames Mutagenicity)	++	+	-	+	—
		0.788	0.646	0.478	0.672	0.236
	Skin sensitization	—	—	—	—	—
		0.288	0.236	0.261	0.293	0.258
	FDAMDD (Maximum Recommended Daily Dose	+	+	+	+	-
		0.668	0.602	0.628	0.544	0.37

Table 5
Prediction of biological activities of bioactives from Himalayan medicinal plants.

Biological Activities	**6, 6′-Biapigenin**		**Candibirin G**		**Candibirin H**		**Catechin 5-*O*-gallate**		**Hypericin**	
	Pa	**Pi**	**Pa**	**Pi**	**Pa**	**Pi**	**Pa**	**Pi**	**Pa**	**Pi**
Membrane integrity agonist	0.946	0.004	–	–	–	–	0.972	0.002	0.889	0.014
Membrane permeability enhancer	0.382	0.067	–	–	–	–	0.233	0.156	0.411	0.052
Membrane permeability inhibitor	0.929	0.003	–	–	–	–	0.652	0.060	0.831	0.006
Anti-inflammatory	0.561	0.040	–	–	–	–	–	–	0.407	0.092
Immunostimulant	0.214	0.122	–	–	–	–	–	–	0.221	0.117
Antitussive	0.308	0.036	–	–	–	–	0.474	0.013	0.178	0.107
Respiratory analeptic	0.374	0.078	–	–	–	–	0.421	0.060	0.284	0.116
SARS treatment	0.328	0.007	–	–	–	–	0.270	0.018	0.216	0.053
Antithrombotic	0.273	0.122	–	–	–	–	–	–	0.220	0.180
Antiinfective	0.466	0.028	–	–	–	–	0.370	0.059	0.486	0.024
Antituberculosic	0.439	0.021	–	–	–	–	0.251	0.109	0.347	0.050
Antiviral (Hepatitis B)	0.479	0.005	0.447	0.009	0.447	0.009	0.283	0.038	0.460	0.008
Antiviral (Influenza)	0.332	0.072	–	–	–	–	0.677	0.007	0.246	0.136
Antiviral (Rhinovirus)	–	–	0.425	0.067	0.425	0.067	0.512	0.020	–	–
Antiviral (Herpes)	0.467	0.014	–	–	–	–	0.454	0.017	0.429	0.024
Biological Activities	**Pseudo hypericin**		**Kaempferol 3-glucoside 7-rhamnoside**		**Kaempferol 7-4-diglucoside**		**Tribuloside**		**Tribulosin**	
	Pa	**Pi**	**Pa**	**Pi**	**Pa**	**Pi**	**Pa**	**Pi**	**Pa**	**Pi**
Membrane integrity agonist	0.840	0.027	0.987	0.001	0.989	0.001	0.996	0.000	–	–
Membrane permeability enhancer	0.372	0.072	0.545	0.007	0.528	0.009	0.386	0.065	0.618	0.003
Membrane permeability inhibitor	0.756	0.019	0.982	0.001	0.978	0.001	0.987	0.000	0.481	0.159
Anti-inflammatory	0.390	0.101	0.724	0.013	0.748	0.010	0.759	0.009	0.757	0.010
Immunostimulant	0.254	0.098	0.611	0.022	0.626	0.020	0.467	0.042	0.567	0.027
Antitussive	0.149	0.143	0.434	0.016	0.571	0.007	0.337	0.029	–	–
Respiratory analeptic	0.222	0.153	0.659	0.018	0.693	0.015	0.506	0.036	0.770	0.010
SARS treatment	0.208	0.061	0.582	0.002	0.661	0.001	0.520	0.003	–	–
Antithrombotic	0.225	0.173	0.643	0.011	0.641	0.012	0.666	0.010	0.596	0.016
Antiinfective	0.417	0.040	0.590	0.005	0.765	0.005	0.483	0.025	–	–
Antituberculosic	0.252	0.107	0.250	0.099	0.456	0.018	0.424	0.025	–	–
Antiviral (Hepatitis B)	0.451	0.009	0.452	0.009	0.484	0.005	0.422	0.012	0.174	0.125
Antiviral (Influenza)	0.251	0.131	0.717	0.005	0.714	0.005	0.667	0.008	0.384	0.052
Antiviral (Rhinovirus)	–	–	–	–	–	–	–	–	–	–
Antiviral (Herpes)	0.431	0.023	0.567	0.005	0.561	0.005	0.539	0.006	0.435	0.022

affirming that these bioactives have firm interactions with the target proteins. Further, the pathway enrichment analysis revealed that pathways related to immunity and apoptosis were common to both HMP bioactive targets and SARS-CoV-2 targets. Thus, it can be said that these HMP bioactives can be used to regulate these pathways by targeting the SARS-CoV-2 proteins. In addition, the selected HMP bioactives were also found to have multiple biological activities, which also enhances their utility against SARS-CoV-2 treatment. However, we have also observed that most of the selected bioactives have poor intestinal and GI absorptions but lower toxicity; therefore, we can adapt different procedures such as nanotechnology, nanoformulation, or pharma-nutraceutical formulation to enhance the absorption of these compounds. By these processes, we can improve the efficacy and reduce the off-target effects of HMP bioactives. Hence, the current study warrants further investigations to test the *in vitro* and *in vivo* effects of the selected HMP bioactives against the SARS-CoV-2 infection.

Funding

The current research work did not receive any specific grant from funding agencies in the public, commercial, or not-for-profit sectors.

Declaration of competing interest

The authors declare that they have no known competing financial interests or personal relationships that could have appeared to influence the work reported in this paper.

Acknowledgment

JN acknowledges research fellowships from the DBT, Govt. of India. PM and BK acknowledge research fellowships from the UGC and CSIR, respectively. AAAS acknowledges the MAHE intramural research grant (MAHE/DREG/PhD/IMF/2019). We also acknowledge CSIR-CFTRI for the support and infrastructure facility.

Appendix A. Supplementary data

Supplementary data to this article can be found online at https://doi.org/10.1016/j.compbiomed.2021.104383.

References

[1] B. Hu, H. Guo, P. Zhou, Z.L. Shi, Characteristics of SARS-CoV-2 and COVID-19, Nat. Rev. Microbiol. 19 (3) (2020) 141–154, https://doi.org/10.1038/s41579-020-00459-7.

[2] P. V'kovski, A. Kratzel, S. Steiner, H. Stalder, V. Thiel, Coronavirus biology and replication: implications for SARS-CoV-2, Nat. Rev. Microbiol. 19 (3) (2020) 155–170, https://doi.org/10.1038/s41579-020-00468-6.

[3] J. Shang, G. Ye, K. Shi, Y. Wan, C. Luo, H. Aihara, Q. Geng, A. Auerbach, F. Li, Structural basis of receptor recognition by SARS-CoV-2, Nature 581 (7807) (2020) 221–224, https://doi.org/10.1038/s41586-020-2179-y.

[4] Y. Wan, J. Shang, R. Graham, R.S. Baric, F. Li, Receptor recognition by the novel coronavirus from wuhan: an analysis based on decade-long structural studies of SARS coronavirus, J. Virol. 94 (7) (2020), https://doi.org/10.1128/jvi.00127-20 e00127-20.

[5] J. Lan, J. Ge, J. Yu, S. Shan, H. Zhou, S. Fan, Q. Zhang, X. Shi, Q. Wang, L. Zhang, X. Wang, Structure of the SARS-CoV-2 spike receptor-binding domain bound to the ACE2 receptor, Nature 581 (7807) (2020) 215–220, https://doi.org/10.1038/s41586-020-2180-5.

[6] D. Wrapp, N. Wang, K.S. Corbett, J.A. Goldsmith, C.L. Hsieh, O. Abiona, B. S. Graham, J.S. McLellan, Cryo-EM structure of the 2019-nCoV spike in the prefusion conformation, Science 367 (6483) (2020) 1260–1263, https://doi.org/10.1126/science.aax0902.

[7] S. Xia, M. Liu, C. Wang, W. Xu, Q. Lan, S. Feng, F. Qi, L. Bao, L. Du, S. Liu, C. Qin, F. Sun, Z. Shi, Y. Zhu, S. Jiang, L. Lu, Inhibition of SARS-CoV-2 (previously 2019-nCoV) infection by a highly potent pan-coronavirus fusion inhibitor targeting its spike protein that harbors a high capacity to mediate membrane fusion, Cell Res. 30 (4) (2020) 343–355, https://doi.org/10.1038/s41422-020-0305-x.

[8] M. Merad, J.C. Martin, Pathological inflammation in patients with COVID-19: a key role for monocytes and macrophages, Nat. Rev. Immunol. 20 (6) (2020) 355–362, https://doi.org/10.1038/s41577-020-0331-4.

[9] H. Ge, X. Wang, X. Yuan, G. Xiao, C. Wang, T. Deng, Q. Yuan, X. Xiao, The epidemiology and clinical information about COVID-19, Eur. J. Clin. Microbiol. Infect. Dis. 39 (6) (2020) 1011–1019, https://doi.org/10.1007/s10096-020-03874-z.

[10] D.B.A Narayana, C.K. Katayar, N.B. Brindavanam, Original system: search, research or re-search, IDMA Bull. 29 (17) (1998) 413–416.

[11] B. Ballabh, O.P. Chaurasia, Traditional medicinal plants of cold desert Ladakh-Used in treatment of cold, cough and fever, J. Ethnopharmacol. 112 (2) (2007) 341–349, https://doi.org/10.1016/j.jep.2007.03.020.

[12] G.M. Morris, D.S. Goodsell, M.E. Pique, W. Lindy Lindstrom, R. Huey, S. Forli, W. E. Hart, S. Halliday, R. Belew, A.J. Olson, Autodock4 and AutoDockTools4: automated docking with selective receptor flexiblity, J. Comput. Chem. 30 (16) (2009) 2785–2791, https://doi.org/10.1002/jcc.21256.

[13] Z. Jin, X. Du, Y. Xu, Y. Deng, M. Liu, Y. Zhao, B. Zhang, X. Li, L. Zhang, C. Peng, Y. Duan, J. Yu, L. Wang, K. Yang, F. Liu, R. Jiang, X. Yang, T. You, X. Liu, X. Yang, F. Bai, H. Liu, X. Liu, L.W. Guddat, W. Xu, G. Xiao, C. Qin, Z. Shi, H. Jiang, Z. Rao, H. Yang, Structure of Mpro from COVID-19 virus and discovery of its inhibitors, Nature 582 (7811) (2020) 289–293, https://doi.org/10.1038/s41586-020-2223-y.

[14] M. Yuan, N.C. Wu, X. Zhu, C.C.D. Lee, R.T.Y. So, H. Lv, C.K.P. Mok, I.A. Wilson, A highly conserved cryptic epitope in the receptor binding domains of SARS-CoV-2 and SARS-CoV, Science 368 (6491) (2020) 630–633, https://doi.org/10.1126/science.abb7269.

[15] P. Towler, B. Staker, S.G. Prasad, S. Menon, J. Tang, T. Parsons, D. Ryan, M. Fisher, D. Williams, N.A. Dales, M.A. Patane, M.W. Pantoliano, ACE2 X-ray structures reveal a large hinge-bending motion important for inhibitor binding and catalysis, J. Biol. Chem. 279 (17) (2004) 17996–18007, https://doi.org/10.1074/jbc.M311191200.

[16] H.M. Berman, J. Westbrook, Z. Feng, G. Gilliland, T.N. Bhat, H. Weissig, I. N. Shindyalov, The protein Data Bank, Nucleic Acids Res. 28 (1) (2000) 235–242, https://doi.org/10.1093/nar/28.1.235. www.rcsb.org.

[17] Y. Gao, L. Yan, Y. Huang, F. Liu, Y. Zhao, L. Cao, T. Wang, Q. Sun, Z. Ming, L. Zhang, J. Ge, L. Zheng, Y. Zhang, H. Wang, Y. Zhu, C. Zhu, T. Hu, T. Hua, B. Zhang, X. Yang, J. Li, H. Yang, Z. Liu, W. Xu, L.W. Guddat, Q. Wang, Z. Lou, Z. Rao, Structure of the RNA-dependent RNA polymerase from COVID-19 virus, Science 368 (6492) (2020) 779–782, https://doi.org/10.1126/science.abb7498.

[18] S. Choudhary, Y.S. Malik, S. Tomar, Identification of SARS-CoV-2 cell entry inhibitors by drug repurposing using in silico structure-based virtual screening approach, Front. Immunol. 11 (2020) 1664, https://doi.org/10.3389/fimmu.2020.01664.

[19] S. Ahmad, Y. Waheed, S. Ismail, S. Bhatti, S.W. Abbasi, K. Muhammad, Structure-based virtual screening identifies multiple stable binding sites at the RecA domains of SARS-CoV-2 helicase enzyme, Molecules 26 (5) (2021) 1446.

[20] S.K. Singh, A.K. Upadhyay, M.S. Reddy, Screening of potent drug inhibitors against SARS-CoV-2 RNA polymerase: an in silico approach, 3 Biotech 11 (2) (2021) 93, https://doi.org/10.1007/s13205-020-02610-w.

[21] E. Pitsillou, J. Liang, K. Ververis, K.W. Lim, A. Hung, T.C. Karagiannis, Identification of small molecule inhibitors of the deubiquitinating activity of the SARS-CoV-2 papain-like protease: in silico molecular docking studies and in vitro enzymatic activity assay, Front. Chem. 8 (2020) 623971, https://doi.org/10.3389/fchem.2020.623971.

[22] J. Natesh, P. Mondal, D. Penta, A.A. Abdul Salam, S.M. Meeran, Culinary spice bioactives as potential therapeutics against SARS-CoV-2: computational investigation, Comput. Biol. Med. 128 (2021) 104102, https://doi.org/10.1016/j.compbiomed.2020.104102.

[23] P. Mondal, J. Natesh, A.A. Abdul Salam, S. Thiyagarajan, S.M. Meeran, Traditional medicinal plants against replication, maturation and transmission targets of SARS-CoV-2: computational investigation, J. Biomol. Struct. Dyn. (2020) 1–18, https://doi.org/10.1080/07391102.2020.1842246.

[24] O. Trott, A.J. Olson, AutoDock Vina: improving the speed and accuracy of docking with a new scoring function, efficient optimization, and multithreading, J. Comput. Chem. 31 (2) (2009) 455–461, https://doi.org/10.1002/jcc.21334.

[25] S. Vardhan, S.K. Sahoo, In silico ADMET and molecular docking study on searching potential inhibitors from limonoids and triterpenoids for COVID-19, Comput, Biol. Med. 124 (2020) 103936, https://doi.org/10.1016/j.compbiomed.2020.103936.

[26] A.T. Onawole, T.U. Kolapo, K.O. Sulaiman, R.O. Adegoke, Structure based virtual screening of the Ebola virus trimeric glycoprotein using consensus scoring, Comput. Biol. Chem. 72 (2018) 170–180, https://doi.org/10.1016/j.compbiolchem.2017.11.006.

[27] D. Gfeller, A. Grosdidier, M. Wirth, A. Daina, O. Michielin, V. Zoete, SwissTargetPrediction: a web server for target prediction of bioactive small molecules, Nucleic Acids Res. 42 (W1) (2014) W32–W38, https://doi.org/10.1093/nar/gku293.

[28] B. Chakrabarty, D. Das, G. Bulusu, A. Roy, Network-based analysis of fatal comorbidities of COVID-19 and potential therapeutics, ChemRxiv (2020), https://doi.org/10.26434/chemrxiv.12136470.

[29] P. Zhou, X. Lou Yang, X.G. Wang, B. Hu, L. Zhang, W. Zhang, H.R. Si, Y. Zhu, B. Li, C.L. Huang, H.D. Chen, J. Chen, Y. Luo, H. Guo, R. Di Jiang, M.Q. Liu, Y. Chen, X. R. Shen, X. Wang, X.S. Zheng, K. Zhao, Q.J. Chen, F. Deng, L.L. Liu, B. Yan, F. X. Zhan, Y.Y. Wang, G.F. Xiao, Z.L. Shi, A pneumonia outbreak associated with a new coronavirus of probable bat origin, Nature 579 (7798) (2020) 270–273, https://doi.org/10.1038/s41586-020-2012-7.

[30] M.V. Kuleshov, M.R. Jones, A.D. Rouillard, N.F. Fernandez, Q. Duan, Z. Wang, S. Koplev, S.L. Jenkins, K.M. Jagodnik, A. Lachmann, M.G. McDermott, C. D. Monteiro, G.W. Gundersen, A. Ma'ayan, Enrichr: a comprehensive gene set enrichment analysis web server 2016 update, Nucleic Acids Res. 44 (W1) (2016) W90–W97, https://doi.org/10.1093/nar/gkw377.

[31] E.Y. Chen, C.M. Tan, Y. Kou, Q. Duan, Z. Wang, G.V. Meirelles, N.R. Clark, A. Ma'ayan, Enrichr: interactive and collaborative HTML5 gene list enrichment analysis tool, BMC Bioinf. 14 (2013) 128, https://doi.org/10.1186/1471-2105-14-128.

[32] A. Chatr-Aryamontri, A. Ceol, D. Peluso, A. Nardozza, S. Panni, F. Sacco, M. Tinti, A. Smolyar, L. Castagnoli, M. Vidal, M.E. Cusick, G. Cesareni, VirusMINT: a viral protein interaction database, Nucleic Acids Res. 37 (Database) (2009) D669–D673, https://doi.org/10.1093/nar/gkn739.

[33] X. Gao, B. Qin, P. Chen, K. Zhu, P. Hou, J.A. Wojdyla, M. Wang, S. Cui, Crystal structure of SARS-CoV-2 papain-like protease, Acta Pharm. Sin. B. 11 (1) (2020) 237–245, https://doi.org/10.1016/j.apsb.2020.08.014.

[34] T. Klemm, G. Ebert, D.J. Calleja, C.C. Allison, L.W. Richardson, J.P. Bernardini, B. G. Lu, N.W. Kuchel, C. Grohmann, Y. Shibata, Z.Y. Gan, J.P. Cooney, M. Doerflinger, A.E. Au, T.R. Blackmore, G.J. Heden van Noort, P.P. Geurink, H. Ovaa, J. Newman, A. Riboldi-Tunnicliffe, P.E. Czabotar, J.P. Mitchell, R. Feltham, B.C. Lechtenberg, K.N. Lowes, G. Dewson, M. Pellegrini, G. Lessene, D. Komander, Mechanism and inhibition of the papain-like protease, PLpro, of SARS-CoV-2, EMBO J. 39 (18) (2020), e106275, https://doi.org/10.15252/embj.2020106275.

[35] Y.M. Baez-Santos, A.M. Mielech, X. Deng, S. Baker, A.D. Mesecar, Catalytic function and substrate specificity of the papain-like protease domain of nsp3 from the Middle East respiratory syndrome coronavirus, J. Virol. 88 (21) (2014) 12511–12527, https://doi.org/10.1128/jvi.01294-14.

[36] A.A. Elfiky, SARS-CoV-2 RNA dependent RNA polymerase (RdRp) targeting: an in silico perspective, J. Biomol. Struct. Dyn. (2020) 1–9, https://doi.org/10.1080/07391102.2020.1761882.

[37] A.K. Byrd, K.D. Raney, Protein displacement by an assembly of helicase molecules aligned along single-stranded DNA, Nat. Struct. Mol. Biol. 11 (6) (2004) 531–538, https://doi.org/10.1038/nsmb774.

[38] M.U. Mirza, M. Froeyen, Structural elucidation of SARS-CoV-2 vital proteins: computational methods reveal potential drug candidates against main protease, Nsp12 polymerase and Nsp13 helicase, J. Pharm. Anal. 10 (4) (2020) 320–328, https://doi.org/10.1016/j.jpha.2020.04.008.

[39] S.K. Patel, J.A. Juno, W.S. Lee, K.M. Wragg, P.M. Hogarth, S.J. Kent, L.M. Burrell, Plasma ACE2 activity is persistently elevated following SARS-CoV-2 infection: implications for COVID-19 pathogenesis and consequences, Eur. Respir. J. 2003730 (2021).

[40] J. Barnes, L.A. Anderson, J.D. Phillipson, St John's wort (Hypericum perforatum L.): a review of its chemistry, pharmacology and clinical properties, J. Pharm. Pharmacol. 53 (5) (2001) 583–600, https://doi.org/10.1211/0022357011775910.

[41] R.S. Baric, Emergence of a highly fit SARS-CoV-2 variant, N. Engl. J. Med. 383 (27) (2020) 2684–2686.

[42] M.I. Khan, Z.A. Khan, M.H. Baig, I. Ahmad, A.E.A. Farouk, Y.G. Song, J.J. Dong, Comparative genome analysis of novel coronavirus (SARS-CoV-2) from different geographical locations and the effect of mutations on major target proteins: an in silico insight, PloS One 15 (9) (2020), e0238344, https://doi.org/10.1371/journal.pone.0238344.

[43] S. Wu, C. Tian, P. Liu, D. Guo, W. Zheng, X. Huang, Y. Zhang, L. Liu, Effects of SARS-CoV-2 mutations on protein structures and intraviral protein–protein interactions, J. Med. Virol. 93 (4) (2020) 2132–2140, https://doi.org/10.1002/jmv.26597.

[44] J.M. Grimes, K.V. Grimes, p38 MAPK inhibition: a promising therapeutic approach for COVID-19, J. Mol. Cell. Cardiol. 144 (2020) 63–65, https://doi.org/10.1016/j.yjmcc.2020.05.007.

[45] H. Tsoi, L. Li, Z.S. Chen, K.F. Lau, S.K.W. Tsui, H.Y.E. Chan, The SARS-coronavirus membrane protein induces apoptosis via interfering with PDK1PKB/Akt signalling, Biochem. J. 464 (3) (2014) 439–447, https://doi.org/10.1042/BJ20131461.

[46] Y. Zhou, T.K. Frey, J.J. Yang, Viral calciomics: interplays between Ca2+ and virus, Cell Calcium 46 (1) (2009) 1–17, https://doi.org/10.1016/j.ceca.2009.05.005.

[47] E.M. De Francesco, V. Vella, A. Belfiore, COVID-19 and diabetes: the importance of controlling RAGE, Front. Endocrinol. 11 (2020) 526, https://doi.org/10.3389/fendo.2020.00526.

[48] T. Thomas, D. Stefanoni, J.A. Reisz, T. Nemkov, L. Bertolone, R.O. Francis, K. E. Hudson, J.C. Zimring, K.C. Hansen, E.A. Hod, S.L. Spitalnik, A. D'Alessandro, COVID-19 infection alters kynurenine and fatty acid metabolism, correlating with IL-6 levels and renal status, JCI Insight 5 (14) (2020), e140327, https://doi.org/10.1172/JCI.INSIGHT.140327.

[49] M.A. Martinez, Compounds with therapeutic potential against novel respiratory 2019 coronavirus, Antimicrob. Agents Chemother. 64 (5) (2020), https://doi.org/10.1128/AAC.00399-20 e00399-20.

[50] P. Glue, R.P. Clement, Cytochrome P450 enzymes and drug metabolism - basic concepts and methods of assessment, Cell, Mol. Neurobiol. 19 (3) (1999) 309–323, https://doi.org/10.1023/A:1006993631057.

[51] D. Thomas, C. Karle, J. Kiehn, The cardiac hERG/IKr potassium channel as pharmacological target: structure, function, regulation, and clinical applications, Curr. Pharmaceut. Des. 12 (18) (2006) 2271–2283, https://doi.org/10.2174/138161206777585102.